Consolidation of surface charging analyses on the Ariel payload dielectrics in the early transfer orbit and L2 space environments

M. Focardi, M. Michelagnoli, M. Pudney, I. Renouf, P. Merola, L. Carbonaro, V. Noce, M. Vela Nunez, P. Bolli, R. Nesti, S. Chiarucci, G. Dinuzzi, E. Tommasi, F. De Persio, M. Salatti, D. Brienza, R. Piazzolla, G. Morgante, E. Pace, G. Preti, G. Micela, G. Malaguti, A. Caldwell, P. Eccleston, G. Tinetti

Published version information:

Citation: M. Focardi et al., Consolidation of surface charging analyses on the Ariel payload dielectrics in the early transfer orbit and L2 space environments, Proceedings Volume 13092, Space Telescopes and Instrumentation 2024: Optical, Infrared, and Millimeter Wave; 1309250 (2024)

DOI: https://doi.org/10.1117/12.3017998

Consolidation of surface charging analyses on the Ariel Payload dielectrics in the early transfer orbit and L2 space environments

M. Focardi[*a,b], M. Michelagnoli[b], M. Pudney[c], I. Renouf[c], P. Merola[a], L. Carbonaro[a], V. Noce[a], M. Vela Nunez[a], P. Bolli[a], R. Nesti[a], S. Chiarucci[a], G. Dinuzzi[a,d], E. Tommasi[e], F. De Persio[e], M. Salatti[e], D. Brienza[e], R. Piazzolla[e], G. Morgante[f], E. Pace[b], G. Preti[b], G. Micela[g], G. Malaguti[f], A. Caldwell[h], P. Eccleston[h], G. Tinetti[i]

and the
Ariel Mission Consortium (AMC)

[a]INAF/OAA - Osservatorio Astrofisico di Arcetri, Largo E. Fermi 5, 50125 Firenze, Italia
[b]Università degli Studi di Firenze - Dip. di Fisica e Astronomia, Via Sansone, 1, 50019 Sesto Fiorentino, Firenze, Italia
[c]AIRBUS Defence and Space, Stevenage, SG1 2AS, UK
[d]INAF/IAPS - Istituto di Astrofisica e Planetologia Spaziali, Via del Fosso del Cavaliere 100, 00133 Roma, Italia
[e]ASI - Agenzia Spaziale Italiana, Via del Politecnico, 00133 Roma, Italia
[f]INAF/OAS - Osservatorio di Astrofisica e Scienza dello Spazio di Bologna, Via Piero Gobetti 93/3, 40129 Bologna, Italia
[g]INAF - Osservatorio Astronomico di Palermo, Piazza del Parlamento 1, 90134 Palermo, Italia
[h]UK-STFC, RAL Space - Rutherford Appleton Laboratory, OX11 0QX Harwell Oxford, UK
[i]University College of London – Dept. of Physics and Astronomy, Gower Street, London WC1E 6BT, UK

ABSTRACT

Ariel (Atmospheric Remote Sensing Infrared Exoplanet Large Survey) [1] [2] is the fourth Mission (M4) of the ESA's Cosmic Vision Program 2015-2025, selected in March 2018 and officially adopted in November 2020 by the Agency, whose aim is to characterize the atmospheres of hundreds of diverse exoplanets orbiting nearby different types of stars and to identify the key factors affecting the formation and evolution of planetary systems. The Mission will have a nominal duration of four years and a possible extension of two years at least. Its launch is presently scheduled for mid 2029 from the French Guiana Space Centre in Kourou on board an Ariane 6.2 launcher in a dual launch configuration with Comet Interceptor.

The baseline operational orbit of the Ariel is a large amplitude halo orbit around the second Lagrangian (L2) virtual point located along the line joining the Sun and the Earth-Moon system at about 1.5 million km (~236 R_E) from the Earth in the anti-Sun direction. Ariel's halo orbit is designed to be an eclipse-free orbit as it offers the possibility of long uninterrupted observations in a fairly stable environment (thermal, radiation, etc.). An injection trajectory is foreseen with a single passage through the Van Allen radiation belts (LEO, MEO and GEO near-Earth environments). This is approximated by a worst-case half orbit, prior the injection and transfer to L2, with a duration of 10.5 hours, a perigee of 300 km (LEO), an apogee of 64000 km (GEO and beyond), and an inclination close to 0 degrees.

During both the injection trajectory and the final orbit around L2, Ariel will encounter and interact mainly with the Sun radiation and the space plasma environment. In L2 the Ariel spacecraft will spend most of its time in the direct solar wind and the Earth's magnetosheath with passages through the magnetotail. These three environments, along with LEO and GEO, can lead to the build-up of a net electric charge on the spacecraft and payload conductive and dielectric

[*]mauro.focardi@inaf.it; phone +39 055 2752 260

Space Telescopes and Instrumentation 2024: Optical, Infrared, and Millimeter Wave, edited by Laura E. Coyle, Shuji Matsuura, Marshall D. Perrin, Proc. of SPIE Vol. 13092, 1309250 · © 2024 SPIE · 0277-786X · doi: 10.1117/12.3017998

surfaces leading to the risk of Electro Static Discharges (ESD), potentially endangering the whole Payload integrity and telecommunications to Ground.

Keywords: Exoplanets, Transit Spectroscopy, Primary and Secondary Eclipses, Atmospheres, Dielectrics Charging, ESD

1. INTRODUCTION

Ariel is the ESA Cosmic Vision M4 Mission whose aim is to characterize the atmospheres of hundreds of diverse exoplanets orbiting nearby different types of stars and to identify the key factors affecting the formation and evolution of planetary systems. Ariel will be the first mission dedicated to the study of chemical composition and thermal structures of atmospheres of hundreds of planets orbiting different types and spectral classes of parent stars and will thus provide a complete picture of the nature of the exoplanets relating it to the planetary bulk parameters and the type and chemical environment of the host star. By performing a large chemical composition survey, Ariel will thus open a new perspective on exoplanet demographics.

Many data regarding the chemical structure of exoplanetary atmospheres have already been collected, both from ground-based facilities and space; however, their statistics are insufficient to draw consistent conclusions on their formation and evolution.

To fulfil the science requirements, Ariel has been specifically designed to implement a stable payload and satellite platform (relying on the L2 environment) optimized to provide a broad, instantaneous wavelength coverage to detect many molecular species, probe the atmospheric thermal structure, identify/characterize clouds and monitor the stellar activity.

2. ARIEL PAYLOAD DESIGN OVERWIEV

The Ariel Payload is conceived modular by design (refer to Figure 1). The adopted baseline architecture splits the payload into two major sections, the cold payload module (PLM) and the items of the payload hosted within the spacecraft service module (SVM), i.e. the warm electronics units.

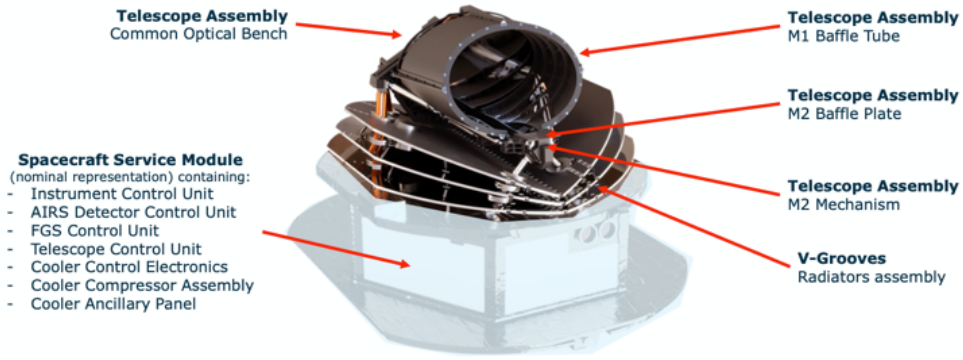

Figure 1: Illustration of the Ariel Payload Module (PLM, top) and Service Module (SVM, bottom) composing the whole Spacecraft (courtesy ADS – AIRBUS Defence and Space).

The SVM houses all the necessary avionic units for spacecraft operation and maintaining the payload under nominal operating conditions. It is composed of a main body enclosed by a top and a bottom sandwich panel made of CFRP (Carbon Fiber Reinforced Plastic) face sheets and aluminum honeycomb. The main body contains all the spacecraft (S/C) avionic equipment and the warm payload (P/L) units while the bottom panel hosts all the equipment that needs to be pointed towards the Sun or the Earth, such as the solar panels, the communication antenna, and the propulsion thrusters activated by the on-board Attitude and Orbit Control System (AOCS) in closed-loop with the Payload's Fine Guidance System (FGS).

The PLM is supported by three bipods mounted onto the Payload Interface Panel (PIP). They are hollow cylinders, made of CFRP (Carbon Fiber Reinforced Polymer) filled with low thermally conductive rigid foam. Three Planck-like V-Grooves (VGs) are adopted as high-efficiency passive radiant coolers, providing the first stage of the PLM cooling system. VGs are made by a simple honeycomb structure of aluminum alloy, thermally connected to the three bipods (to intercept the conducted parasitic heat leaks through the mounting bipods) and are mechanically supported and thermally decoupled from the PIP by GFRP (Glass Fiber Reinforced Polymer) struts.

The telescope, part of the TA (Telescope Assembly) [3], is based on a Cassegrain design with a parabolic primary (M1) and a hyperbolic secondary mirror (M2) plus a third mirror M3 used to re-collimate the beam. A fourth mirror M4 directs the collimated beam onto the optical bench, within the Instrument Cavity (IC) where a common optics and dichroics set is located in order to feed the Ariel IR Spectrometer (AIRS) and FGS optical modules. M2 is supported by a refocusing mechanism with three degrees of freedom (focus and tip/tilt). The purpose is to correct for one-off movements due to launch loads and cool-down and potentially to make occasional adjustments (for example to compensate for any long-term drifts in structural stability). As M2 is moved, also the position of the star (and its spectrum) moves on AIRS and FGS field of view (FoV). Because FGS closes the AOCS loop, this ensures that the star is kept onto the spectrometer slit at all times during any focusing operation.

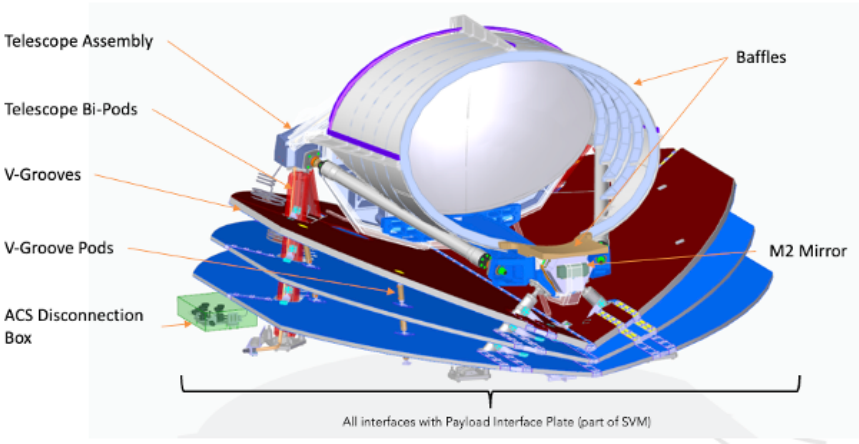

Figure 2: The Ariel cold Payload section (PLM) front view.

The telescope optical system directs the M3 collimated beam, which is split into different wavelengths by dichroics and common optics, feeding the two separate instruments with overlapping fields of view:

- The Fine Guidance System [4] [5], whose job is to ensure the centering, focusing, and guiding of the satellite and providing high-precision photometry of the target in the visible band and a low resolution near-IR spectrometer. To accomplish these functions, the FGS instrument will be equipped with two detectors operating in four spectral bands: FGS–1 [0.6-0.8 μm], FGS–2 [0.81-1 μm], VISPhot [0.50-0.60 μm] and NIRSpec [1.10-1.95 μm]. The data produced by the FGS-1 and FGS-2 channels will be redundant and will be used both for photometric analysis and to generate redundant guiding information to the S/C by providing the centroid position of the target star at 10 Hz. Data from the FGS detectors are collected by the FPE (Focal Plane Electronics) working at 137 K as operational temperature and hosting two SIDECAR ASICs for the IR (HgCdTe-based) detectors. The FPE is supported by insulating GFRP-based struts mounted on the Telescope optical bench.
- The Ariel IR Spectrometer [7] [8], which provides low-resolution spectroscopy in two IR channels: AIRS-Ch0 [1.95-3.90 μm] with $R \geq 100$ and AIRS-Ch1 [3.90-7.80 μm] with $R \geq 30$. AIRS is located at the intermediate focal plane of the telescope and optical system common to the two instruments. It hosts two Teledyne IR detectors based on ternary compounds of Mercury, Cadmium, and Tellurium (HgCdTe) sensitive to the wavelengths of interest and two analog interface electronics, the so-called Cold Front-End Electronics (CFEE), cooled to 55 K, for the management and reading of the detectors. The system consisting of the detector and reading electronics is managed by a control unit (AIRS Detector Control Unit or A-DCU) which in turn is managed by the Instrument Control Unit (ICU) [9] [10] [11] of the PLM.

For the S/C thermal control, a combination of two cooling systems will be used:

- A passive cooling system, as anticipated, consisting of a series of V-Groove radiators, a high-efficiency thermal shielding system that isolates the P/L module from the spacecraft bus. It will allow the P/L to cool down to a temperature of approximately 55 K, in the L2 environment, while the SVM nominal temperature will be kept in the range 253 K - 323 K.
- An Active Cooler System (ACS) with a Joule – Thomson effect compressor for the active cooling, through compression and expansion of Neon gas, of the AIRS detectors which will operate at cryogenic temperatures, close to 42 K.

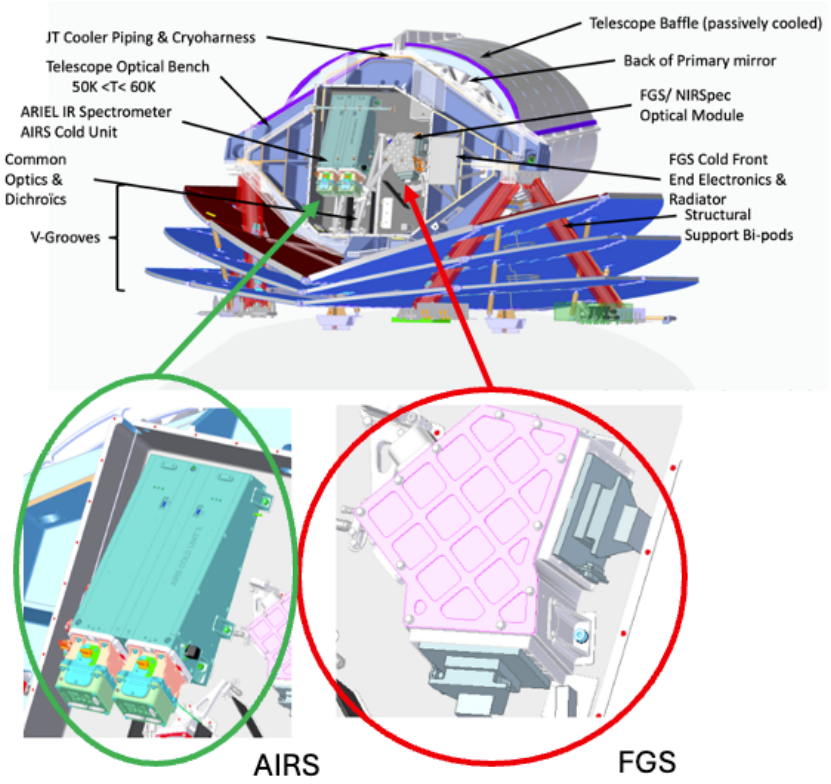

Figure 3: The Ariel cold Payload section (PLM) rear view showing the Instrument Cavity (IC) content and a magnification of AIRS and FGS enclosures here located.

The Ariel S/C is designed in such a way as to ensure that the Sun will never illuminate the cryogenic PLM in all operational conditions. This is achieved by defining a correct S/C design and geometry using the SVM and solar panels to shield the PLM during all the operational phases.

3. ARIEL ORBIT

The baseline operational orbit of the Ariel spacecraft is a large amplitude halo orbit around L2, an unstable point of equilibrium in the Sun-Earth-Moon gravitational system. This point is inferred from the Circular Restricted Three-Body Problem which returns five equilibrium points, of which three are unstable, including L2. The L2 virtual point is located along the line joining the Sun and the Earth-Moon system at about 1.5 million km (~236 R_E) from the Earth in the anti-Sun direction and is becoming the orbit of choice of many current (e.g. JWST) and future (e.g. PLATO) astronomical missions because it offers the possibility of long uninterrupted observations in a fairly stable environment. To guarantee this feature, the Ariel halo orbit is designed to be an eclipse-free orbit allowing for a simple design of the communications and power subsystems due to stable distances to the Earth and Sun and a consistent Sun-Spacecraft-Earth angle. Additionally, it offers a low-risk radiation environment in contrast to near-Earth orbits crossing the radiation belts as described in the following sections.

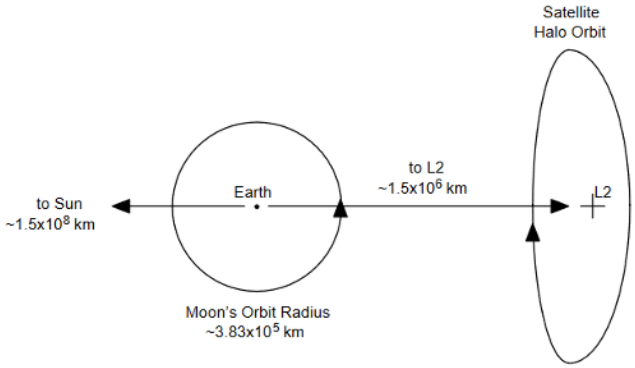

Figure 4: Ariel halo orbit around L2 with no eclipses allowed during the mission lifetime.

The Ariel SC will be launched, along with the Comet Interceptor Mission, around local noon by an Ariane A6.2 rocket with its Dual Launch Structure (DLS) from Kourou, in the French Guiana. A direct escape orbit injection is planned in the baseline mission profile, being characterized by and involving different plasma environments.

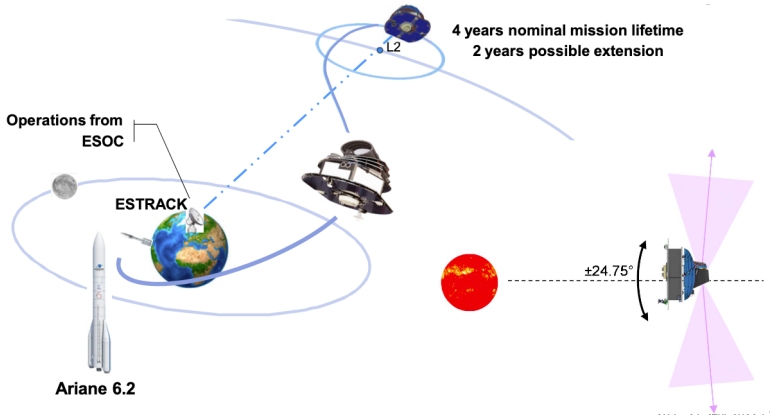

Figure 5: The Ariane 6.2 launch vehicle will inject Ariel into a direct transfer towards the libration point L2 of the Sun-Earth system. Launches to L2 will naturally be around noon local time of the perigee, since the apogee is towards the anti-Sun direction.

The injection trajectory to L2 (transfer orbit) is foreseen with a single passage through the Van Allen radiation belts and different Earth Orbits altitudes. This is approximated by a worst-case half orbit with a duration of 10.5 hours, perigee 300 km (LEO) and apogee 64000 km (GEO). An inclination close to 0 degrees is assumed as a worst case, so a transient geostationary orbit will be considered instead of a geosynchronous one, as assumption for the charging simulations. After 30 days, the transfer phase concludes, marking the beginning of the commissioning and, then, science operations.

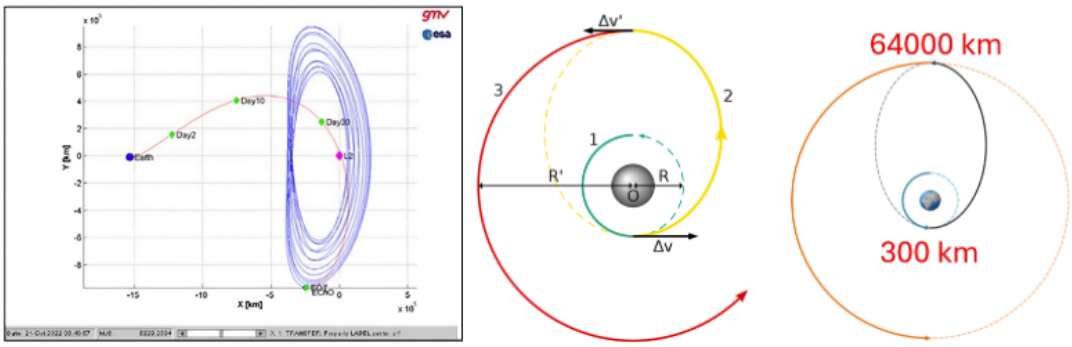

Figure 6: Left: Example of Ariel injection and final orbit around L2. The blue point represents the Earth, the green points represent, respectively, day 2, day 10, and day 30 from the lift-off, and the pink one the L2 point. Right: Half orbit with perigee in LEO (green orbit 1) and apogee at GEO (red orbit 3) and LEO to GEO intermediate transfer trajectory (yellow 2).

The ascent trajectory foresees the fairing jettison after about 4 minutes from the lift-off at about 100-150 km of altitude, exposing the S/C to the surrounding plasma and the Earth's thermosphere environment. During this time, the S/C will be in a virtual eclipse as it will still be attached to the S/C Dual Launch Structure (DLS) and in its shadow. After about one hour from the lift-off, at about 10000 km of altitude, the S/C will detach from the DLS, exposing Ariel solar panels to the direct solar light while maintaining the cryogenic P/L always in the SVM shadow [12].

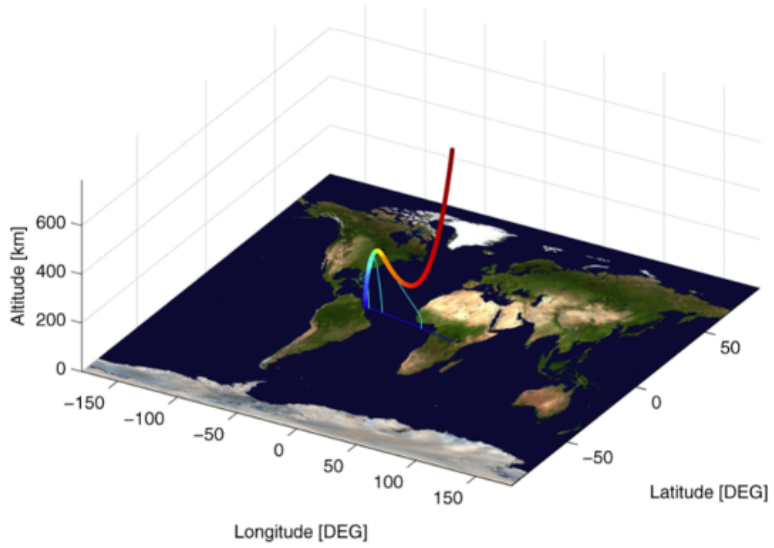

Figure 7: Direct ascent trajectory for a direct L2 transfer injection without intermediate low-Earth parking orbit. The trajectories of the sub-orbital parts are depicted in cyan.

During the transfer phase and because of the amplitude of the final halo orbit around L2, the Ariel S/C will spend most of its time in the direct solar wind and the Earth's magnetosheath and a small fraction of time in the Earth's magnetotail environment.

The natural environment related to the interplanetary plasma includes gravitational fields due to the Earth, Moon, Sun, and planets; plasma, magnetic fields, and energetic charged particles connected to both the solar wind and the Earth's magnetospheric tail; shocked plasma, magnetic fields, and energetic charged particles of the magnetosheath at the boundary region between free solar wind and the magnetospheric tail; galactic cosmic rays; electromagnetic radiation and thermal conditions due to the emitted energy from the Sun, as well as meteoroids from both the sporadic background and streams. It is worth noting that spacecraft, Ariel included, interact constantly with electromagnetic (EM) radiation (e.g. light, interplanetary EM waves, not intentional and intentional RF-waves for communication to ground, etc.), charged particles (electrons, protons, and heavy ions) from the plasma environment, and Galactic Cosmic Rays (GCRs).

Since the environment near the second Lagrangian point is characterized by many processes, including charging, that may compromise the nominal spacecraft operations, it is important to put some effort into maximizing the system robustness by a proper materials and coatings choice along with grounding and bonding of subsystems to the S/C chassis.

3.1 Plasma environments

Low Earth Orbits (LEOs) mark the inner limit of the inner radiation belt and are orbits that extend up to a few hundred km over the sea level and are usually not of concern for spacecraft charging, except for passages through the auroral zones where severe charging events may occur; however, as the injection orbit is assumed as a nearly 0-degrees inclination orbit, even a milder environment is foreseen. At these altitudes, the ambient plasma is usually characterized by high density (of the order 10^5 cm^{-3} or higher for the dayside while lower for the nightside) and low energy (usually below a few eV). In this environment, the S/C surfaces usually charge to very low levels because when a surface gets slightly charged, charges of opposite sign are quickly attracted neutralizing the formerly formed one. This is possible thanks to the high density of the environment plasma, smaller Debye lengths and relevant electrostatic sheaths.

As anticipated, after 213.5 seconds (less than 4 minutes) from the Ariel launch, as reported by the ESA's CREMA (Consolidated Report on Mission Analysis) [12] document, fairing jettison occurs, at about 100 – 150 km of altitude, exposing the S/C to the surrounding plasma. As a result of Ariel shared launch with Comet Interceptor, the spacecraft is sun-shielded by the Dual Launch adapter/Structure (DLS) throughout the launcher ascent phase, eliminating the need to account for illumination constraints (i.e. direct illumination). However, after the separation, at about 10000 km altitude, the S/C is directly exposed to direct sunlight affecting the charging balance by photoelectron emission. After the separation from the DLS, the satellite bends eastward and the panels, along with the entire S/C, are oriented towards the sun to start charging the onboard batteries and shielding the PLM from direct solar illumination.

In LEO, up to an altitude of about 1000 km, satellites travel at an orbital velocity of approximately 8 km/s and take about 90 minutes to complete one orbit. Therefore, for the entire time required to cover ~1000 km in LEO (a few minutes, accounting for the launcher accelerating ascent), the drift velocity vector of the plasma is directed from the telescope towards the solar panels.

The plasma density parameters adopted for the charging simulations have been retrieved by the reference Ariel Environment Specification document from ESA [14] and ECSS [15], assuming a somewhat worst-case scenario in which the S/C is found at a solar magnetic local time equal to 18:00 h, i.e. in dusk. On the night side, the plasma density (particle cm^{-3}) at such altitudes is reduced as the atmosphere is not exposed to EUV radiation leading thus to a decrease in ions and electrons production (photoionization) and favoring the recombination of charged particles, especially the heavier ions. This represents a somewhat worst-case scenario as a lower plasma density leads to a lesser mitigation of the S/C charging phenomenon, as it can also be inferred from Figure 8 where, from an altitude of about 6500-7000 to 10000 km (where the Ariane 6.2 DLS release is expected) and beyond, the surface charging hazard become serious for a shadowed spacecraft orbiting close to the equator.

In addition, for near-Earth environments, at altitudes above 400 km and as a function of latitude (higher than 35 degrees and up to an altitude of about 7000 km and beyond), a high spacecraft charging hazard can occur.

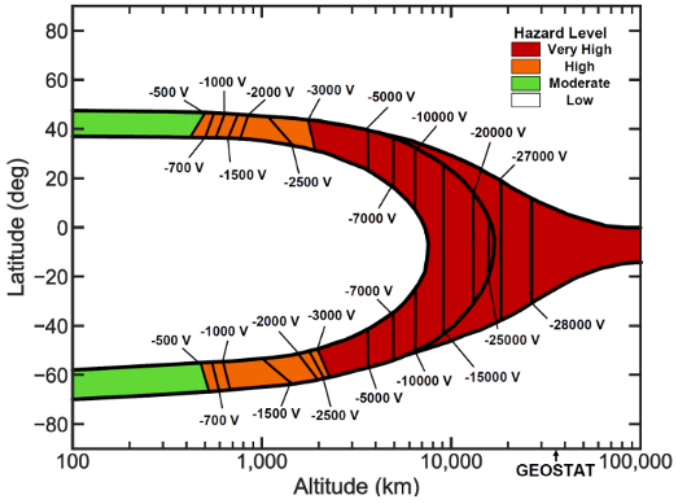

Figure 8: Near-Earth zones of concern for Surface Charging Hazards for a shadowed spacecraft. It is clearly shown that for LEO orbits near the Equator a low risk related to surface charging is foreseen, while for GEO orbits high levels of surface potential are expected. Data based on Defense Meteorological Satellite Program (DMSP – 800 km) and Freja Observations.

The geostationary orbit (GEO) environment is instead characterized by lower plasma densities and dominated by energetic electrons and ions leading to strong time variations. Since high energy electrons are the main cause of S/C charging, this phenomenon often takes place heavily with respect to other environments, negatively charging the S/C surfaces to hundreds of volts or even several kV if the S/C is not exposed to direct sunlight, where the photoemission current can contribute to the total current balance. This is indeed one of the most common regions where spacecrafts are affected by spacecraft charging, as it has been experienced by many satellites that have been flown until now.

The outer GEO orbits mark the upper limit of the outer radiation belt and start merging with the Earth's magnetotail and magnetosheath, before being limited by the bow shock and the external solar wind.

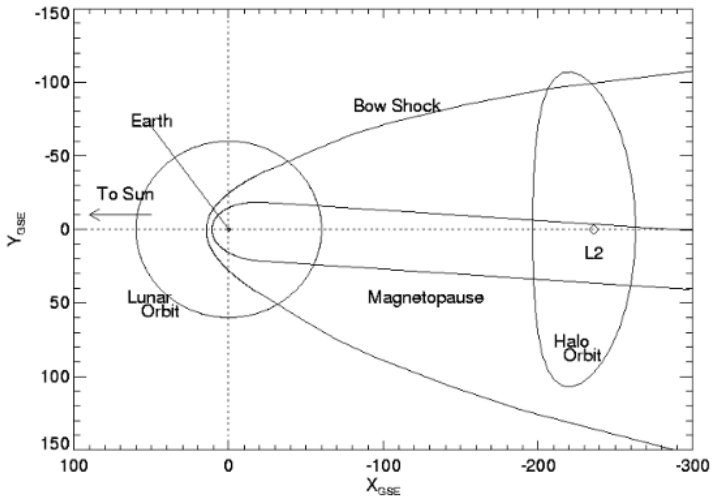

Figure 9: Earth-Moon System, Magnetotail, Magnetopause, Bow Shock and Halo Orbit around L2

The magnetotail, if compared to the solar wind and the magnetosheath, contains low-density and high-temperature plasma. To date, it is not yet completely clear how far the Earth's magnetotail extends but, thanks to the data collected so far, we are able to state that it extends well beyond L2. The magnetotail is a complex and dynamic structure with size and orientation determined by many factors as the solar wind velocity and dynamic pressure, the strength and direction

of the interplanetary magnetic field, and the orientation of the Earth's magnetic axis. Around L2 the magnetotail can be approximated to a cylinder with a radius of about 20-30 R_E.
Beyond approximately 50 R_E, the plasma in the magnetotail is substantially solar wind plasma that entered the tail by means of the dayside polar cusp or locally along the open magnetopause boundary. Generally, the bulk flow velocity is lower than the solar wind one but with a generally anti-sunward component although in specific conditions it can give a general sunward component.
The orientation of the magnetotail is determined by its interaction with the solar wind and more specifically by its direction. Because of this, the Earth's magnetotail orientation is highly variable, reaching an aberration angle from the Sun-Earth line up to about 10° (15° extreme) with an average of about 4°, as shown in Figure 10. Assuming, therefore, that L2 is always located in the magnetotail is erroneous because its interaction with the solar wind regularly moves the magnetotail far from the Sun-Earth direction. This means that Ariel's orbit can pass through the magnetotail if the aberration angle is large enough. The aberration angle is reduced during periods of increased wind pressure, as can happen, for instance, during periods of maximum solar activity; while large aberration angles can manifest during transient solar wind disturbances. As the Ariel S/C will operate during a solar minimum period, it is not improbable that the mission will encounter the magnetotail environment.

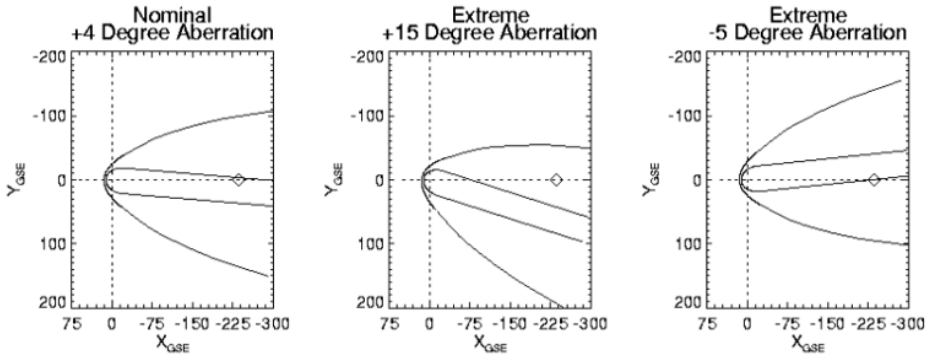

Figure 10: Magnetotail aberration angle. As can be infer from the extreme degree aberration, Ariel orbit can meet the Magnetotail environment.

The Earth's magnetosheath consists mainly of shocked solar wind plasma that has been diverted around the magnetosphere. Its outer boundary is the bow shock formed where the supersonic solar wind flow is abruptly decelerated as a consequence of its interaction with the Earth's magnetosphere, while its inner boundary is the magnetopause. Once the solar wind plasma crosses the bow shock, its forward motion is converted into thermal energy, leading to a temperature increase. Furthermore, as the plasma slows down, stagnating and building up in the subsolar region in front of the magnetosphere, its density increases.
Data collected to date allow to state that the magnetosheath plasma density is greater than the magnetotail plasma density while the electron and ion temperatures are relatively low compared to the magnetotail environment. This allows to infer that the magnetosheath is mainly an area of relatively high density and low energy plasma. As the plasma in the magnetosheath is of solar origin, its composition is close to the solar wind plasma. The bulk flow velocity is always antisunward as the plasma flows around the magnetopause in the same way as the free solar wind flow. Because solar wind conditions are variable, magnetosheath dimensions are variable as well. As a direct consequence, the magnetosheath orientation is highly variable meaning that the Ariel S/C can result in the direct solar wind, in the magnetotail, or the magnetosheath. Around L2 the magnetosheath radius is of the order 100 R_E.

Finally, the solar wind is a continuous but variable flow of plasma and magnetic fields released from the Sun. It is produced, accelerated and heated from the corona fields, the Sun's outer atmosphere and its origin must be sought in the corona's high temperature that causes it to expand against the solar gravity force. The solar wind is thus an outflow of coronal material that starts from the base of the corona, where the pressure is high, with essentially a null macroscopic velocity, and gets accelerated outwards where the pressure is lower.
The solar wind is generated near the Sun as hot, dense, and slow-moving plasma which gets accelerated outward and becomes cool, rare, and supersonic near Mercury and beyond. As most of the solar wind acceleration takes place close to

the Sun surface, the Ariel S/C will not be affected by significative velocity variations as its distance from the Sun varies too little to be able to experience any direct effect.
The solar wind time-scale variation ranges from tens of minutes to days, small respect to the orbital period of the Ariel S/C around L2 (about 180 days ~6 months), meaning that the S/C may encounter several different plasma regimes within a single orbit. The physical characteristics of the solar wind show a recurrence of approximately 27 days, corresponding to the solar rotation period. Furthermore, the solar wind physical parameters vary cyclically with an average period of 11 years, corresponding to the duration of the solar cycle.
Close to the Earth, the presence of the planet's magnetic field causes the supersonic solar wind to suddenly decelerate generating the bow shock, i.e. a shock wave where the solar wind gets slowed, compressed, heated, and deflected.
The solar wind is mainly composed of electrons and protons with Helium the most abundant minor species. Ions that are heavier than Helium are still present in the solar wind but their contribution to the solar wind density is negligible. The same composition can be found in the magnetosheath and, roughly, in the magnetotail at L2 distances as the main plasma source in the magnetotail at distances beyond 100 R_E is the solar wind.
Even though the solar wind plasma is cold, ions may have enough kinetic energy to cause sputtering from surface materials, i.e. typical values are ~1 keV for protons and ~4 keV for He^{++}. In the magnetosheath, the kinetic energy is lower, but sputtering can still occur.
The solar wind velocity at 1 A.U. lies in the range of 300 – 1200 km/s and generally, its mean value is around 400 km/s. The high-speed wind has a mean velocity of about 750 km/s at 1 A.U. from the Sun and originates from zones of the corona characterized by a magnetic topology with open field lines such as high-latitude regions or coronal holes. The slow wind has a typical velocity of about 400 km/s and is generated in zones characterized by closed magnetic field lines such as low-latitude regions. Since the Earth is situated on the ecliptic plane, it is mainly affected by slow wind, although the presence of a coronal hole at lower latitudes can allow fast wind to reach L2 the Earth causing geomagnetic disturbances.
The solar wind plasma regime is thus characterized by a not spherical symmetry, as the polar wind is on average faster and less dense than the equatorial wind; however, for the scopes of this work about Ariel surface charging simulations, only the equatorial wind has been considered.

4. ARIEL CHARGING MODEL VS SPACECRAFT CONFIGURATION

Surface charging simulations have been carried out by means of the SPIS (Spacecraft Plasma Interaction Software) simulator, a complex free tool provided by the SPINE (Spacecraft Plasma Interaction Network in Europe) community [13]. A simplified CAD model of the spacecraft has been adopted due to the memory demand and long computation times necessary for analyses and simulations on complex models. The model is meshed by its partition into discrete geometric and topological cells of triangular (surface) and tetrahedral (bulk) shape, whose material properties are defined by a geometrical editor, as the SPIS software hosts an embedded database that allows to simulate different configurations and materials such as conductors, semiconductors, dielectrics, paints and coatings composing physical groups and complex spacecraft structures.
In addition, SPIS allows to define an internal SPICE-like circuit (netlist) between different structural parts by defining a series of Electrical Super Nodes (ESNs) assigned to physical groups. ESNs can be connected via user-defined impedances or voltage differences (biasing conditions) between them. All potentials (biases) are defined with respect to the spacecraft ground node (chassis) and the computed voltage levels can be plotted with respect to the plasma (baseline) or the spacecraft potential.
SPIS allows to model Secondary Electron Emission (SEE) and photoelectron emission as well as plasma drift velocity effects. For the GEO and the Ariel final halo orbit around L2, the plasma drift velocity dominating factor is commonly the fast drift velocity of the plasma flowing radially away from the Sun, impinging directly on the spacecraft solar array.
In order to keep the number of tetrahedral meshes at a reasonable value, the following simplifications of the geometrical model were made with respect to the more complex Ariel CAD design:

- Radiators: smaller surfaces of similar material on the same flat panel are merged into one single large area, and radiator edges were brought in from the panel edges to allow some space.
- MGA (Medium Gain Antenna): modelled as a simplified thicker metal structure (Al) detached from the main spacecraft body.
- Solar Array and PIP: both use a thicker panel size.

- V-Grooves: modelled with a thicker size and an increased gap between V-Grooves to allow for meshing between them and the PIP.
- Telescope: simplified model detached from the V-Grooves and given sufficient thickness to allow for a reasonable mesh size. Telescope and S/C main body are made equipotential by means of the ESN/SPICE circuit.
- Bipods: shaped so that they do not touch at the top in order to reduce the weight of the mesh. This simplification has minimal impact as all bipods are then grouped into a single ESN. Low resistances are assumed as their interfaces with the telescope and the PIP by means of the ESN/SPICE circuit.
- VGs supporting struts: only six struts are modelled in the geometry and are then grouped into a single ESN. As for the telescope, VGs are considered part of the S/C chassis.
- FPE – IC harness connectors: only one of connector (dielectric part) is modelled due to its reduced dimensions and the need to adopt a suitable meshing.
- FPE struts: only one FPE strut is modelled (same consideration for FPE-IC).

In the following figures the adopted Geometrical Model for the overall spacecraft (warm SVM and cold PLM) is shown. Colors are aligned with those adopted for the retrieved 2D curves (voltage levels).

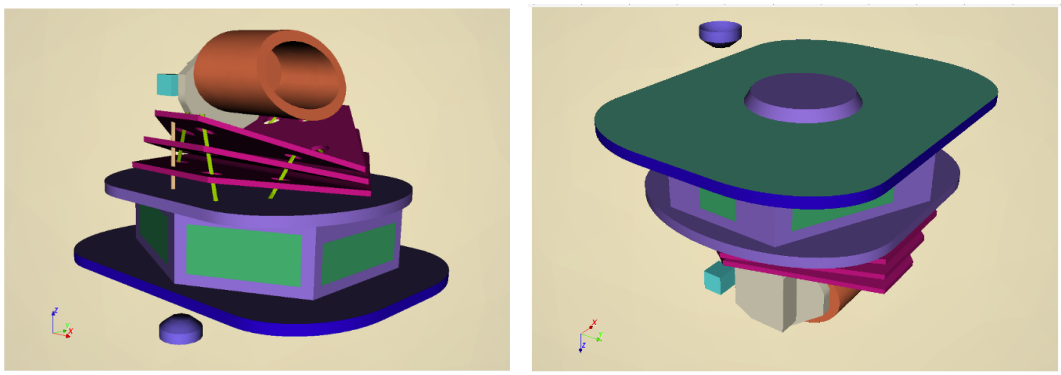

Figure 11: Ariel Geometrical Model used for SPIS simulations. Left: front view; Right: bottom view.

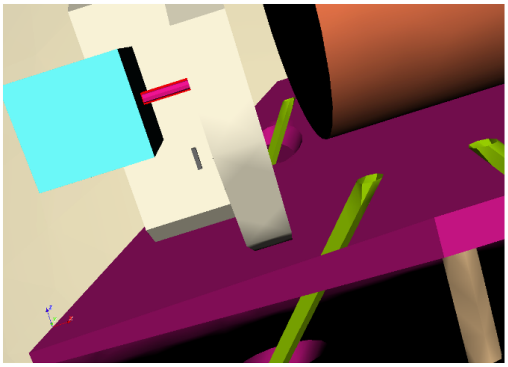

Figure 12: Ariel Geometrical Model used for SPIS simulations (closeup on FPE-IC connector in dark brown and FPE strut in magenta)

Electrical SuperNodes and selected materials are listed in Table 1.

ESN #	Colour		Description	Material	SPIS Adopted Material
0	N/A	N/A	Ground node (virtual node)	N/A	N/A
1		Dark Green	Solar Array Front	Solar Cell	Solar Cell (Cerium doped+MgF2) (125 µm)
2		Liliac	Launcher Adaptation Ring + Main Body + PIP	Carbon Loaded Kapton 160XC (MLI)	Kapton Black (2K) (antistatic polyimide tape)
3		Blue	Solar Array Edges	Exposed Carbon Fibre / Kapton tape edge seal	Epoxy (50 µm) (worst case)
4		Orange	Telescope Baffle	Aluminium	Aluminium (2K)
5		Ivory	Instrument Cavity + TOB	Aluminium (MAP-AQ PUK coating on radiator face)	Aluminium (2K)
6		Cyan	FPE box	Aluminium	Aluminium (2K)
7		Light green	PL Bipods	CFRP	Carbon fibre material properties
8		Pink	V-Grooves	Aluminium	Aluminium (2K)
9		Green	Radiators	White Paint SG121FD	White Paint (PSG121FD 125 µm) (dielectric film)
10		Purple	MGA Antenna	Aluminium	Aluminium (2K)
11		Beige	PL Struts	GFRP	Epoxy material properties
12		Dark Grey	FPE harness connector	Insulator	FPTE/Teflon
13		Pink with red borders	FPE Strut	GFRP	Epoxy material properties
			External boundary		
			Computational volume		

Table 1. Electrical SuperNodes numbering and selected materials.

5. THE SPIS SIMULATOR

The Spacecraft Plasma Interaction Software (SPIS) [13], is a simulation suite based on a numerical kernel, called SPIS-NUM, an electrostatic 3D unstructured Particle-In-Cell (PIC) plasma model consisting of a Java-based highly modular Object-Oriented library. The SPIS simulator provides a friendly user interface called SPIS-UI for easy browsing and accessing to the simulation modules. The SPIS-UI allows the user to easily define all the needed input parameters such as spacecraft geometry, meshes, material properties, boundary conditions, internal circuit and plasma environment parameters. The parameters definition steps correspond to the pre-processing phase. Then, following the SPIS processing phase, at the end of the simulation, the user can access the output data in the dedicated data mining section including physical quantities 2D plots and 3D potential maps by means of the 3D viewer Cassandra.

The modular structure of the software allows to define the simulation parameters in a linear and direct way. A module cannot be accessed until all the previous ones have been set. This has been conceived in order to minimize the risk of errors and corruption of the data model. The modular structure of SPIS allows the user to browse the various panels

during the simulation setting process; however, to avoid data corruption it is recommended by the SPINE community to define all the parameters in a single run in a linear manner.

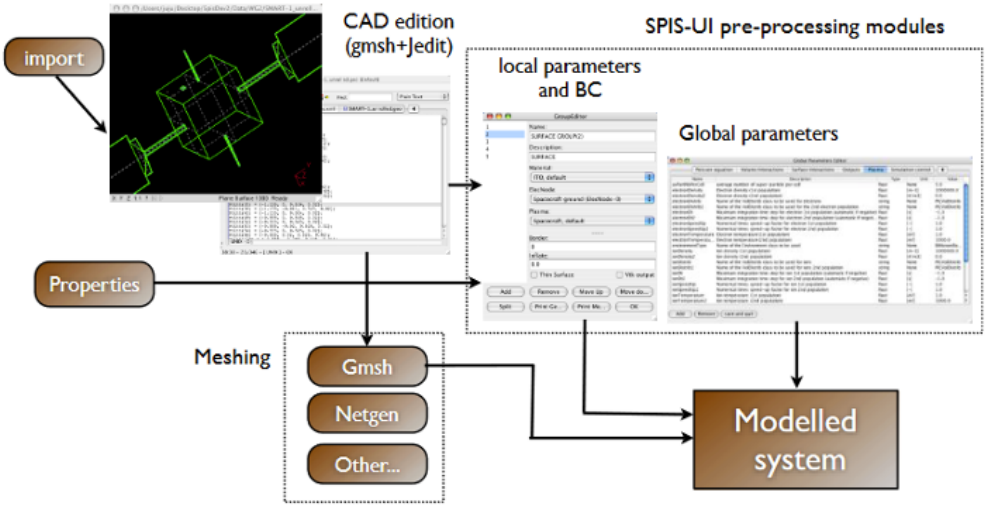

Figure 13: Definition of the model system in the pre-processing phase.

5.1 Geometrical modelling and meshing

For the geometrical modelling of the spacecraft structure, a third-party 3D finite element mesh generator (GMSH) is used as a CAD engine and meshing tool. This tool allows the user to define complex spacecraft 3D structures; however, for the sake of simplicity and to lighten the computational costs, a simplified geometry of the structure is recommended. A complete geometrical system should be constituted of:

- The spacecraft structure, defined by one or more closed surfaces. This corresponds to the inner mathematical boundary. Inside these closed surfaces there is no plasma.
- An external boundary, defined by one closed surface, that should correspond to the external mathematical boundary. This external boundary should be large enough to contain the natural unperturbed environment; that is, it has to be large enough for the perturbation of the natural environment due to the spacecraft to be negligible.
- The computational volume delimited by the above boundaries and in relationship with the Debye length.

After defining the spacecraft geometry, the user needs to mesh it. In GMSH the mesh dimension can be defined individually for each defined geometrical point. To ensure the simulation convergence and accuracy the simpler and low reliable SPIS meshing tool shall never be used, but rather using GMSH directly in which meshing can be optimized and monitored.

5.2 Electrical nodes definition

Spacecraft electrical behavior can be modelled by an electric circuit collecting and emitting currents from and to the plasma. Three different types of electric nodes are defined within SPIS:

- Electrical Super Nodes (ESNs): they are macroscopic nodes defined by the user through SPIS-UI, take part in the internal SPICE netlist, and typically cover a sub-system of the spacecraft. ESNs can be both dielectrics and conductors. If any electrical component connecting them is defined, the ESNs are left floating.
- (Regular) Nodes: when the spacecraft mesh gets uploaded on SPIS, the code automatically generates a node for every surface element. Nodes cannot be modified by the user.

- Reduced Nodes: when a set of different nodes (regular + super nodes) are connected by active biases, a reduced node is generated by the code. Reduced nodes are hidden from the user and cannot be modified.

At code level, the spacecraft model deals with nodes and super nodes (and makes all the generation of nodes and reduced nodes), while the circuit model only works with reduced nodes.
Each electrical node is associated with a subsystem of the S/C for which the materials that compose it must also be defined with their respective characteristics and properties. In SPIS there is an archive with many pre-defined materials, but it is also possible for the user to define them independently and upload them in the simulator.
As can be retrieved from Table 1, each subsystem of the S/C is assigned a material and an ESN with its corresponding ID. This is done by the user via the SPIS-UI in the "Group Editor" panel. The correct definition of the ESNs and the internal circuit definition are crucial for the correct implementation of a simulation.

5.3 Spacecraft Electric Circuit modelling

The electric circuit in SPIS is defined in three steps:

- The coating electrical properties definition which is done in the group editor panel. The user associate material and electrical properties to a surface keeping in mind that depending on the material bulk conductivity (BUC) and surface resistivity (SRE) the equivalent electrical circuit for the coating may differ.
- The spacecraft equivalent circuit, which connects electrical nodes through explicit electrical components that have to be defined by the user by means of a netlist (Equivalent Spice circuit netlist).
- The plasma, which is explicitly simulated by SPIS. It is expressed as a linear component in the SPIS circuit solver by "current scalers" associated to each kind of plasma population distribution model.

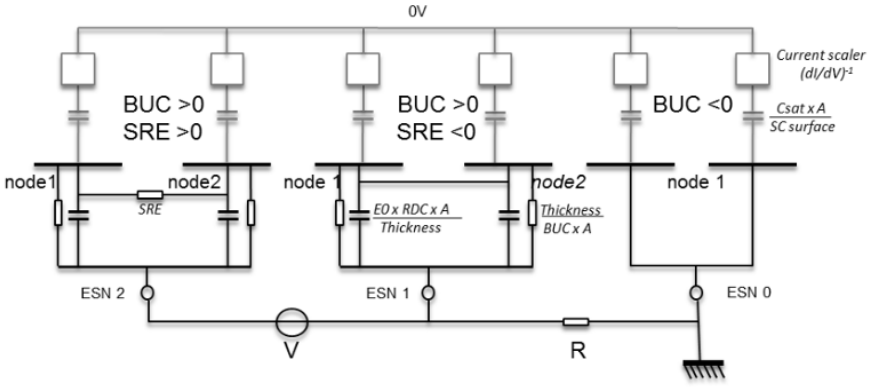

Figure 14: Schematic view of a SPIS equivalent circuit. The top part is the implicit plasma circuit, the middle part is the implicit coating circuit, and the bottom part is the user defined explicit S/C circuit.

In Figure 14, a schematic view of a generic SPIS equivalent circuit is shown. It is worth noting that where BUC (bulk conductivity) is defined negatively, it means that the chosen component is a conductor with no coating. Here, the bottom part corresponds to the user-defined explicit S/C circuit, the middle part is the implicit coating circuit defined in the group editor, and the top part is the implicit plasma circuit defined by means of the global parameter editor.
The potential is defined with respect to the undisturbed plasma while the S/C local ground is referred to as node 0 (a virtual node for the Ariel model, to which the physical S/C chassis node is referred).
Two types of electrical circuit components can be defined:

- Continue/diffuse components: usually represent uniform surface components (e.g. paints and coatings) over a subsystem of the spacecraft whose properties can be inferred by the material properties (lumped constant over a single mesh).
- Discrete components: discrete devices defined by the user in the "Electric circuit editor" panel. They have to be plugged between ESDs.

The code calculates the absolute potential by means of the absolute S/C capacitance with respect to the undisturbed plasma while differential charging is calculated using the dielectric capacitance and resistivity. The S/C capacitance is defined as the ratio of the total charge on an equipotential spacecraft (or S/C chassis, i.e. parts having the same potential reference) to its potential. The S/C capacitance can be figured out as a capacitor plugged between the S/C ground and the plasma located at infinity and its value depends on the plasma conditions. This capacitance is spread over all the S/C local grounds in proportion to their respective areas.

5.4 Equivalent Spice Circuit (Netlist)

The Electric circuit editor is a text editor in which it is possible to enter a SPICE-like netlist defining the electrical connections between different electrical nodes connecting the spacecraft elements. This list is based on the standard SPICE netlist syntax.

5.5 Boundary Conditions (Global Parameters)

The Global Parameters Editor panel allows to define parameters like global physical values of the space environment (e.g. temperature, density, etc.) or numerical values (e.g. simulation duration) that are general to the simulation and have not to be deployed locally on the mesh. Global parameters are divided into many subcategories and are also classified on the basis of the level of familiarity of the operator with respect to the software itself in order to modify them without causing errors or data corruption: the so-called “Verbosity level”. It can be low, medium, advanced, and expert.
Once the environment and the numerical values have been defined in the Global Parameters Editor, the pre-processing phase is almost done. The last step consists in the conversion of the input parameters from the SPIS-UI data structure to the SPIS-NUM one. This action will also build the corresponding numerical model. At this stage, if the simulator provides an error message this means that the system definition is incorrect, and the user has to correct it before running the simulation.

5.6 Plasma Environment Definition and Input Parameters Selection

The second Lagrangian point is sufficiently close to the 1 A.U. environment that plasma parameters for the 1 A.U. case can be usually assumed.

A slightly positively charged S/C is preliminarily expected to be found in L2 as the S/C will be immersed in the low-density solar wind for most of the time and will be exposed (solar arrays) to direct sunlight making the contribution of photoemission dominant. Passages through the Earth’s magnetotail and magnetosheath are also foreseen. In this fairly quiet environment, no risk of ESDs is predicted.

A direct escape injection orbit is planned which involves a single passage through the Van Allen radiation belts, including the LEO and GEO plasma environments. While for the LEO and inner Van Allen radiation belt environment, no particular risk of ESDs is predictable, the GEO plasma environment may generate not negligible voltage differences between the S/C surfaces; especially between the shadowed surfaces and the ones exposed to sunlight.

Ariel’s orbit is structured in such a way that it is never naturally eclipsed by the Earth or the Moon during the various phases, except before the separation of Ariel from the dual launch structure (DLS) causing a virtual shadowing. This phase occurs at approximately 10000 km altitude, therefore a simulation in a LEO environment with the S/C virtually eclipsed (by DLS) is foreseen. Although the LEO environment does not represent a threat from an ESD point of view, transition phases from one environment to another (e.g. from one eclipsed to one exposed to sunlight) may lead to an increasing ESD risk.
The nominal orientation of the S/C with respect to the Sun can be retrieved from Figure 15, showing that Ariel geometry allows to keep the cryogenic PLM always in shadow, while the selected plasma parameters for the performed simulations are listed in Table 2.

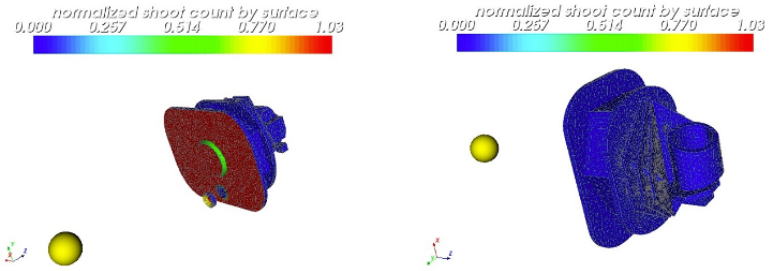

Figure 15: Sun position w.r.t. the S/C showing also the normalized solar flux.

Orbit/Environment →		LEO (shaded)	GEO (sunlight)	Solar Wind (sunlight)	Magnetosheath (sunlight)	Magnetotail (sunlight)
Parameter	**Unit**	**Averaged value at 1 AU**				
Electron Plasma Density	$[cm^{-3}]$	5.31×10^3	10	8.7	1.0	0.11
Proton Plasma Density	$[cm^{-3}]$	4.73×10^3	10	8.31	0.96	0.11
Helium ion Plasma Density	$[cm^{-3}]$	5.46×10^2	N/A	0.39	0.04	N/A
Oxygen ion Plasma Density	$[cm^{-3}]$	3.24×10^1	N/A	N/A	N/A	N/A
Electron energy	[K] [eV]	1.2×10^3 0.1	5.8×10^6 500	1.0×10^5 8.6	3.1×10^5 26.7	21×10^5 181
Proton energy	[K] [eV]	5.8×10^3 0.5	5.8×10^6 500	1.2×10^5 10.3	9.3×10^5 80.2	63×10^5 543
Helium ion energy	[K] [eV]	5.8×10^3 0.5	5.8×10^6 500	5.8×10^5 50	9.3×10^5 80.2	N/A
Oxygen ion energy	[K] [eV]	5.8×10^4 5	N/A	N/A	N/A	N/A
Drift velocity	[km/s]	8	468	468	313	60
Debye length	[m]	0.03	52.6	7.4	38.4	301.5
N_α/N_P	[−]	N/A	N/A	0.047	0.047	N/A

Table 2. Plasma parameters adopted for the simulations.

6. SIMULATION RESULTS

In L2, the ambient plasma has a relatively low density and energy (kinetic velocity), and the S/C is always in sunlight, therefore due to the high levels of photoemission, the emitted current on sunlight surfaces can be higher than the maximum electron current flowing from the plasma to the S/C. This tends to charge the sun-facing S/C surface positively recollecting, as a direct consequence, part of the emitted electrons.

Due to the high numerical density of the plasma particles, their low energy and the shadowed ascent phase up to 10000 km due to the DLS presence prior its release, in LEO the S/C is expected to charge very little since, as soon as it tends to charge by a few volts, it immediately attracts charged particles of the opposite sign, compensating (a small Debye length is expected).

In GEO, however, higher potential levels are expected due to the higher energy (electrons and protons/ions kinetic velocities) of the plasma particles and larger Debye lengths.

During the simulations, the plasma flux is ruled by the injection of charged particles into the boundary surface from randomly chosen locations. The considered environment is modelled by a double Maxwellian with each population that can be represented using a particle approach, the Particle in cell (PIC) or a fluid approach, the Maxwell–Boltzmann one, or a mixed approach with the particle motion used to compute the current and Maxwell–Boltzmann to calculate the density in the computational volume. The Particle-in-Cell (PIC) code uses a number of macroparticles, called superparticles, each of them representing many physical particles, which are integrated according to the equations of motion for charged particles under the action of the electromagnetic (extended Lorentz) force, including both electric and magnetic field, if present. The initial position and velocities of the superparticles are determined using a Monte Carlo technique. The plasma dynamic is ruled by the Vlasov equation. Both electrons and positive ions are modelled by a PIC volume distribution in the L2 environment to obtain more reliable data, even though it is more computationally demanding. For the LEO and GEO simulations, the Maxwellian distribution is used for electrons to reduce the computational cost.

The S/C capacitance is set to 10 μF which is quite large, as usually lower values are more realistic, but it only affects the transient and settling time of the ground potential and does not affect the computed potential levels in steady state conditions, as the actual simulation target. This value also helps to improve the stability of the model and to reduce the computational time.

The duration of the simulation is set in such a way as to find a reasonable compromise between the computational cost (settling time up to steady state included) and the achievement of an equilibrium state. Simulations in the L2 environments have been carried out for 30s while in LEO and GEO, shorter times have been simulated. This is indeed related to the time needed to simulate the plasma dynamics.

6.1 LEO transient (early orbit)

As expected, and as it can be retrieved from Figure 16, the S/C surfaces are only slightly positively charged. This is a direct consequence of the high-density and low-energy plasma present in the LEO environment (compared with GEO and L2) given that, as soon as the S/C becomes slightly charged and accounting for the characteristic Debye length, a large number of charges of opposite sign are immediately attracted and the net charge is reduced to negligible values. As the S/C is artificially shielded by the DLS until about one hour after the launch time and up to a distance of 10000 km at least, the direct photoelectron current from the Ariel spacecraft does not participate in the current balance. Even if the S/C is in eclipse (as a worst-case assumption close to the natural shadowing by the Earth), it is deemed that it starts charging slightly positively (refer to the elapsed time in the X-axis) because the electron population does not have enough energy to reach the critical temperature (kinetic energy) to start the spacecraft negative net charging mechanism.

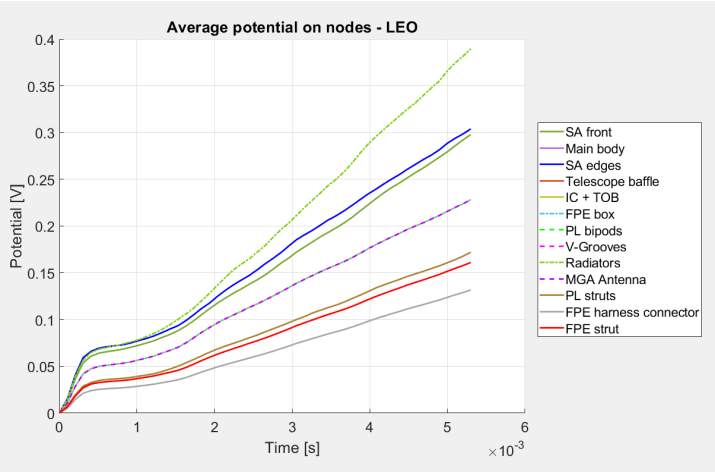

Figure 16: Time dependent surface potential evolution – LEO orbit.

Since literature with discordant parameters regarding the temperature of O+ ions were found, multiple simulations were carried out to verify the different implications regarding the different hypotheses. It has been shown that taking a temperature for O+ ions equal to 5 eV or 0.5 eV does not lead to significant variations in the potential levels reached by the various surfaces. Finally, a simulation with only H+ and He++ ions was performed and also in this case no significant variations were found compared to the previous cases. It is therefore concluded that O+ ions, at such low concentrations, have no significant effects on the charging phenomenon in LEO. In Figure 18 the $\log_{10}$ of the total charge density at t = 0.005 s with a cut through the z-y and the x-z planes has been reported.

The potential differences (mutual between materials and the surrounding plasma) elaborated by SPIS in this environment, of the order of a few tenths of a V, are not cause of concern from an ESD point of view as they are much lower than the threshold value of 100 V imposed as reference by the ECSS [16] and Spacecraft Charging Fundamentals [17]. In any case, a much longer simulation time is required in order to let the SPIS simulator reaching a steady state (plateau) for each voltage level, and this requires a more performant workstation, as this LEO simulation required 20-24 hours.

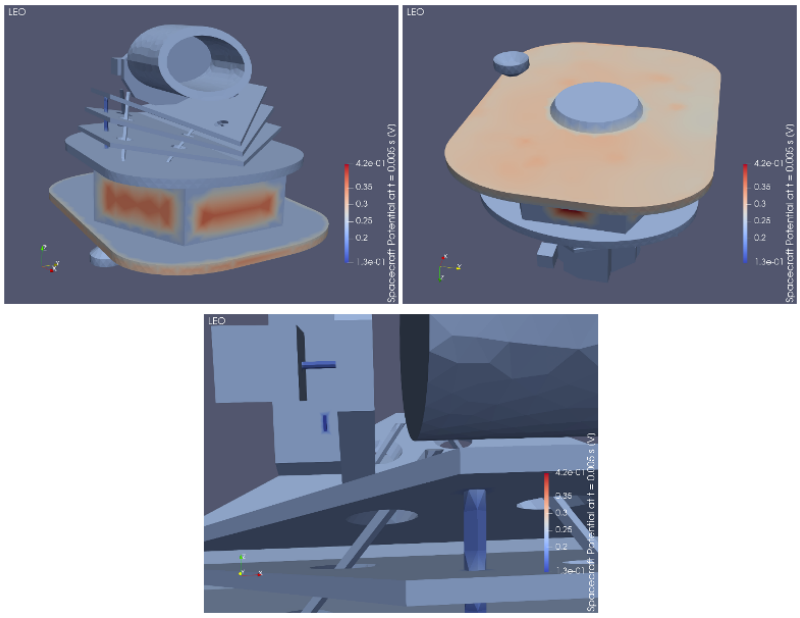

Figure 17: 3D map of spacecraft potential – LEO orbit. First figure: Ariel front; second figure: Ariel bottom; third figure: closeup on FPE-IC connector and FPE strut.

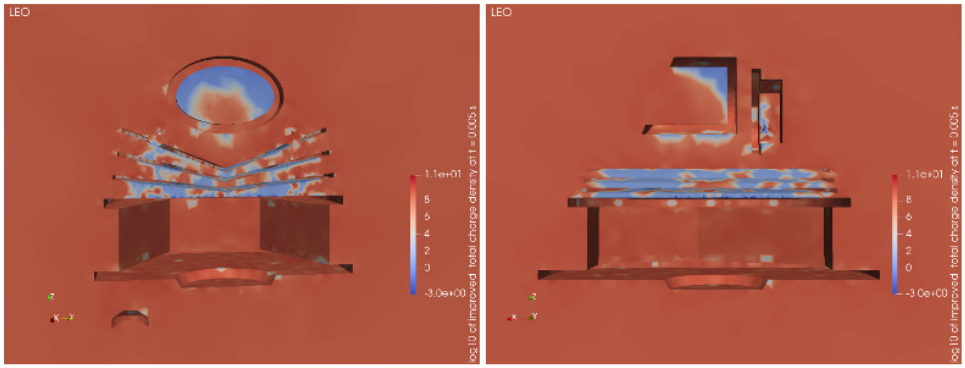

Figure 18: $\log_{10}$ of total charge density (q/m^3) at t = 0.005 s with a cut through the S/C in z-y plane and x-z plane – LEO orbit.

6.2 GEO and early insertion orbit to L2

As anticipated, the GEO orbit is the one of most concern. As inferred from Figure 19, some S/C dielectric surfaces (e.g. radiators, FPE struts, and FPE-IC harness connectors) charge to higher negative potentials albeit the S/C is in sunlight (solar arrays). This is due to the high energy particles present in the GEO environment and much lower densities along with a larger electron flux with respect to the ions flux. In addition, even though the surfaces charge at negative potential levels, high-energy electrons can still reach the S/C surface. Having a larger electron flux with respect to positive ions flux, the surfaces will tend to charge negatively.

As can be seen from Figure 19, the Solar Array front tends firstly to charge positively and then to discharge. This is due to that the S/C is initially immersed in an empty computational volume into which the plasma particles are inserted from the outer edge at the same time as the radiation coming from the Sun is activated. When this happens, the front of the solar panel begins to emit photoelectrons due to the interaction with solar radiation and secondary electrons due to the interaction with the charged particles of the plasma. Because secondary electron emissions can exceed the incoming flow of electrons, especially early on when the surface has not reached a high enough potential to prevent the secondary electrons from drifting away, the surface tends to become positively charged. However, as the surface interacts with other surfaces both through the internal circuit defined with the SPICE netlist and through the generated potential, the surface begins to discharge in the transient. In any case, as for the LEO environment, and accounting for a not fully representative simulation during the transient due to the assumed large S/C capacitance, a much longer simulation time is required in order to let the SPIS simulator reach a steady state (plateau) for each voltage level. It is worth noting again that the plateau is actually the reference voltage at the equilibrium for the simulations target and the performed analyses are limited by the available computational power.

In Figure 21, the $\log_{10}$ of the total charge density at t = 6.0 s with a cut through the z-y and the x-z planes has been reported. The timestamp of the graph is shorted than the actual duration of the simulation because the final graph was corrupted and the uncorrupted time stamp closer to the end of the simulation was taken.

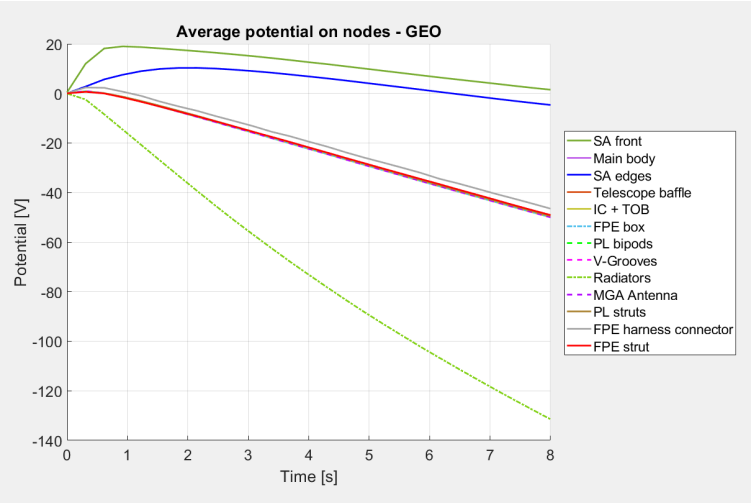

Figure 19: Time dependent surface potential evolution – GEO orbit.

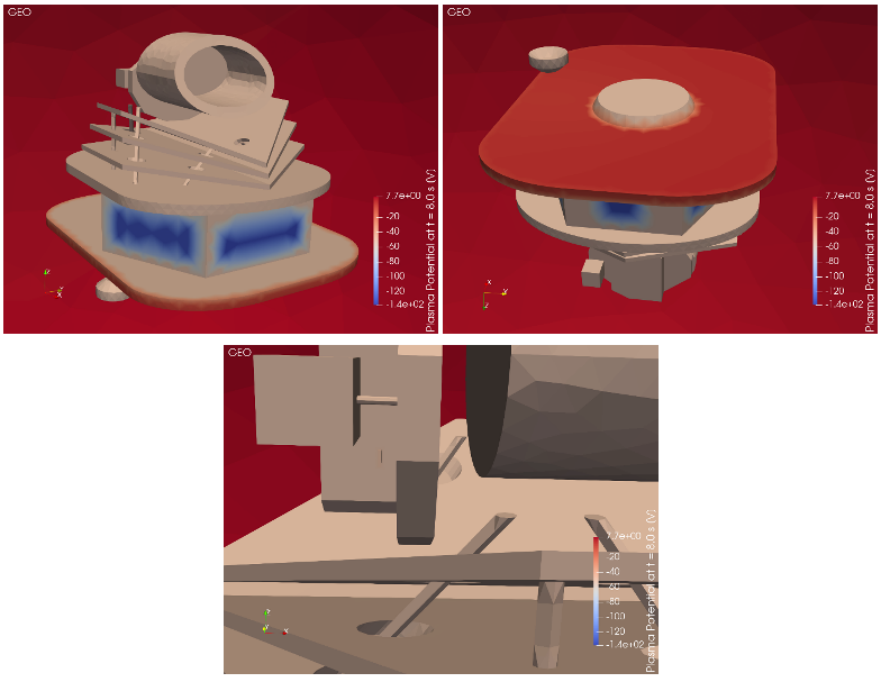

Figure 20: 3D map of plasma potential – GEO orbit. First figure: Ariel front; second figure: Ariel bottom; third figure: closeup on FPE-IC connector and FPE strut.

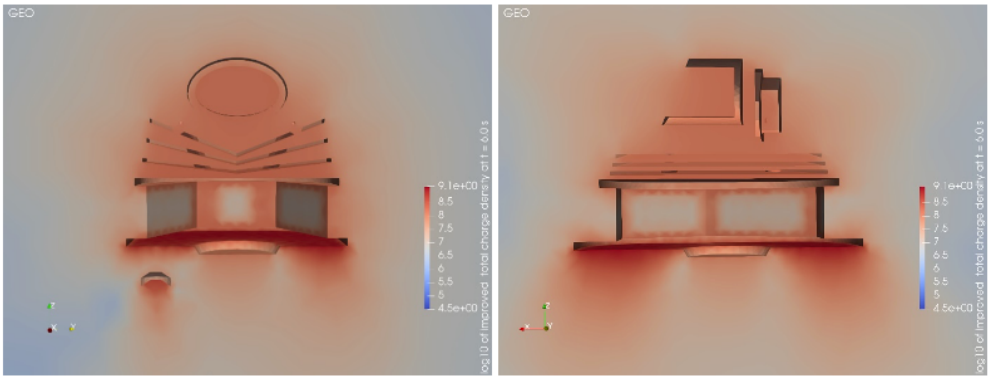

Figure 21: $\log_{10}$ of total charge density (q/m^3) at t = 6.0 s with a cut through the S/C in z-y plane and x-z plane – GEO orbit

In order to better understand how the S/C surfaces exposed to sunlight can negatively charge, the highly negative potential of shadowed surfaces needs to be accounted for. The negative potential contours, extending from the high voltage (dark) side to the low voltage (sunlit) side, create a potential barrier that traps photoelectrons. Given that photoelectrons typically possess only a few eV of energy, a small potential barrier captures the majority of them. Consequently, the suppression of photoemission allows the sunlit side to accumulate high negative potentials. This phenomenon also helps to explain why the solar array front initially charges positively and then moves towards negative potentials along the path to the steady state equilibrium.

The on-board sensitive instrumentation, on the payload side, will be kept off during the insertion orbit towards L2 to avoid any risk of damage and disturbances to the telecommunication (e.g. housekeeping and science telemetries) by potential ESD-related transient electromagnetic waves. However, with absolute voltage differences of the order of hundreds of Volts, the risk of an ESD between two S/C surfaces or from the S/C to the plasma environment does exist. It must be kept in mind that the actual Payload grounding and bonding structures are not fully simulated by the Ariel implementation in SPIS. Furthermore, both the P/L and FPE GFRP struts are actually covered with MAP-PUK AQ black paint to prevent ESDs, not considered in the Ariel SPIS implementation in order to evaluate any related potential drawback on the P/L charging without implementing such a kind of mitigation method.

6.3 1 A.U. Solar Wind

The mean energy of electrons and ions, and the plasma density are lower with respect to the ones in the GEO environment. This allows the S/C surfaces exposed to sunlight to charge positively to about 14.5 V with respect to the plasma level due to photoemission. As for the GEO simulation, the dielectric surfaces firstly charge positively due to the secondary electron emission which has a higher yield for dielectrics than conductors. During the first seconds of simulation, these surfaces do not develop a potential level high enough to reattract the emitted electrons allowing them to leave the surfaces. After a few seconds, the interaction with all the other surfaces causes the potential of these dielectric surfaces to decrease.

The potential differences obtained in this environment are not a cause of concern for the ESDs as the biggest potential difference is about 25 V (between the Solar Array front at about 14.5 V and the radiators that are at about -10.5 V), well below the threshold value of 100 V imposed by the ECSS reference. However, the potential differences that have been established until the steady state is reached may lead to local charging of dielectrics potentially producing not severe ESDs, but able to interfere with on-board instrumentation and, for this reason, further analysis will be required only in case of higher-level of net charging turned out with longer times along with not negligible ESD risk.

As for the GEO environment, this simulation represents a somewhat worst-case scenario without accounting for grounding and bonding structures and with GFRP not covered by conductive MAP-PUK AQ black paint. Simulation for the solar wind case can be deemed more reliable due to that most of the voltage curves reach their plateau as a function of the longer delta-t associated with the characteristic plasma frequencies leading to a computing simplification so that longer simulations (order of 30 s) can be performed for a comparable timeframe of 16-20 hours.

In Figure 24 the $\log_{10}$ of the total charge density at t = 30.0 s with a cut through the z-y and the x-z planes has been reported.

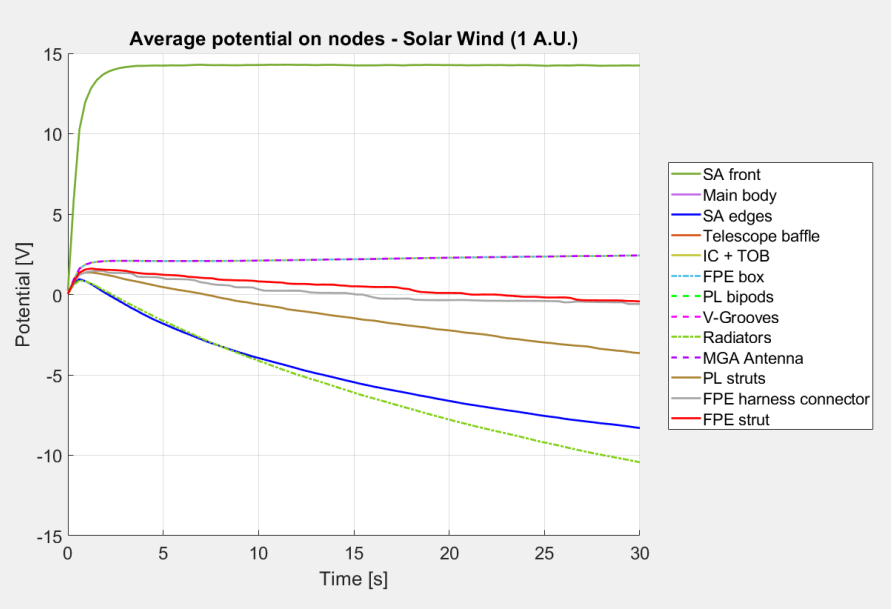

Figure 22: Time dependent surface potential evolution – Solar Wind (1 A.U.).

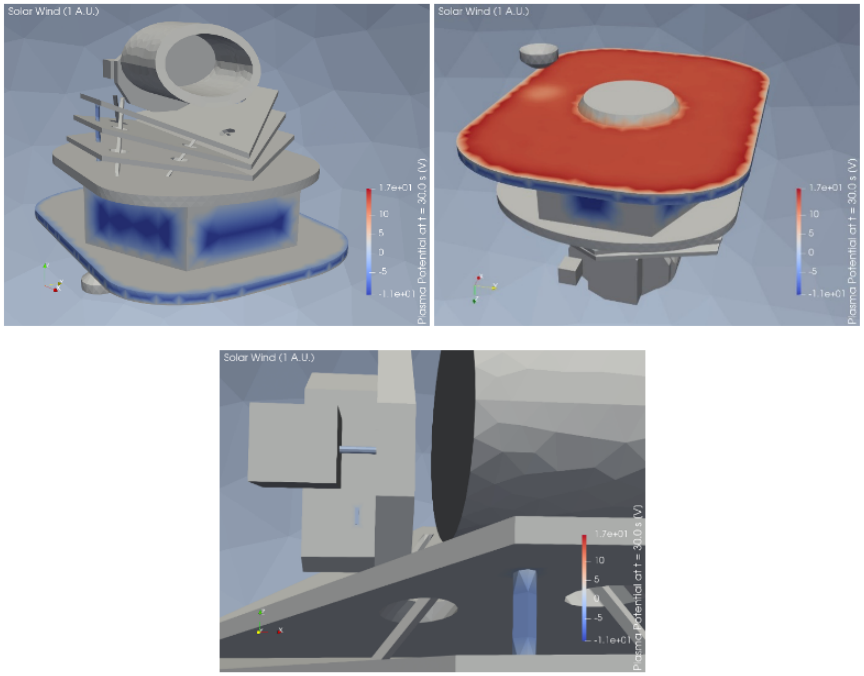

Figure 23: 3D map of plasma potential – Solar Wind (1 A.U.). First figure: Ariel front; second figure: Ariel bottom; third figure: closeup on FPE-IC connector and FPE strut.

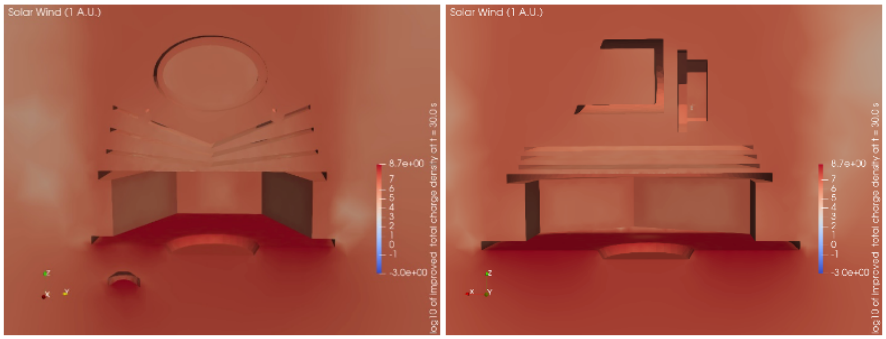

Figure 24: $\log_{10}$ of total charge density (q/m^3) at t = 30.0 s with a cut through the S/C in z-y plane and x-z plane – Solar Wind.

6.4 1 A.U. Magnetosheath

The different plasma environment with respect to the Solar Wind case, causes the S/C surfaces to charge as can be seen in Figure 25. As the plasma is less dense and more energetic, the potential of the exposed surface is higher with respect to the Solar Wind case. More energetic charged particles can pass through the potential barrier generated by surfaces charged with the same sign getting thus collected by the same. Less density means also less particles attracted by oppositely charged surfaces that could balance the formed net charge. Moreover, accounting for a more energetic plasma than the solar wind environment, we get closer to the energy at which there is maximum secondary emission of electrons, thus increasing the number of electrons that can be emitted.

In this environment, the potential differences obtained are not a cause of concern for the ESDs as the biggest potential difference is about 20 V between the Solar Array front, at about 19 V, and the Solar Array edges, at about -1.0 V. However, such voltage differences could interfere with on-board instruments as above described, and further analysis will be required for longer times in order to let the curves reaching their plateau.

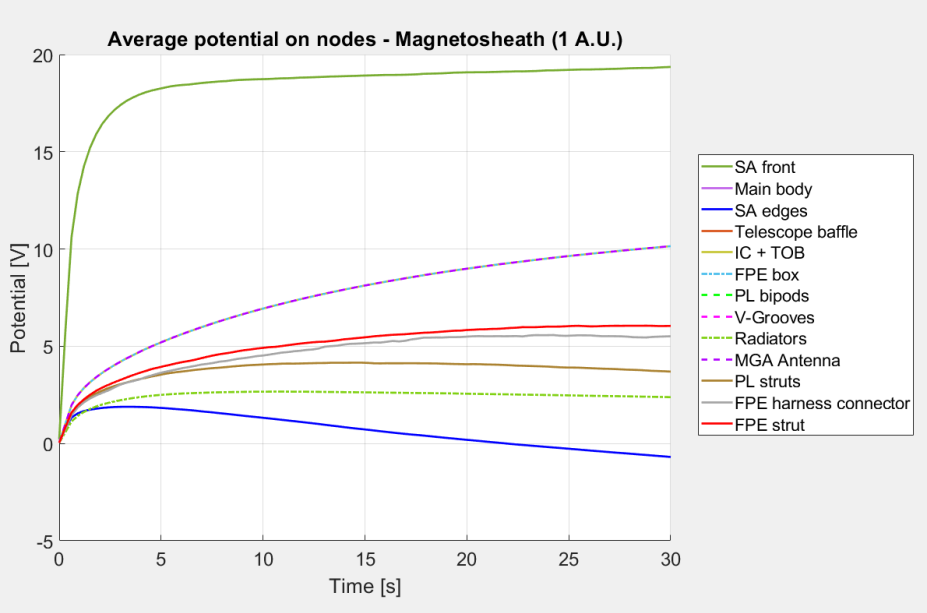

Figure 25: Time dependent surface potential evolution – Magnetosheath (1 A.U.).

As for the previous cases, this simulation represents a somewhat worst-case scenario without grounding and bonding structures, and with GFRP not covered by conductive MAP-PUK AQ black paint.

In Figure 27 the $\log_{10}$ of the total charge density at t = 30.0 s with a cut through the z-y and the x-z planes has been reported.

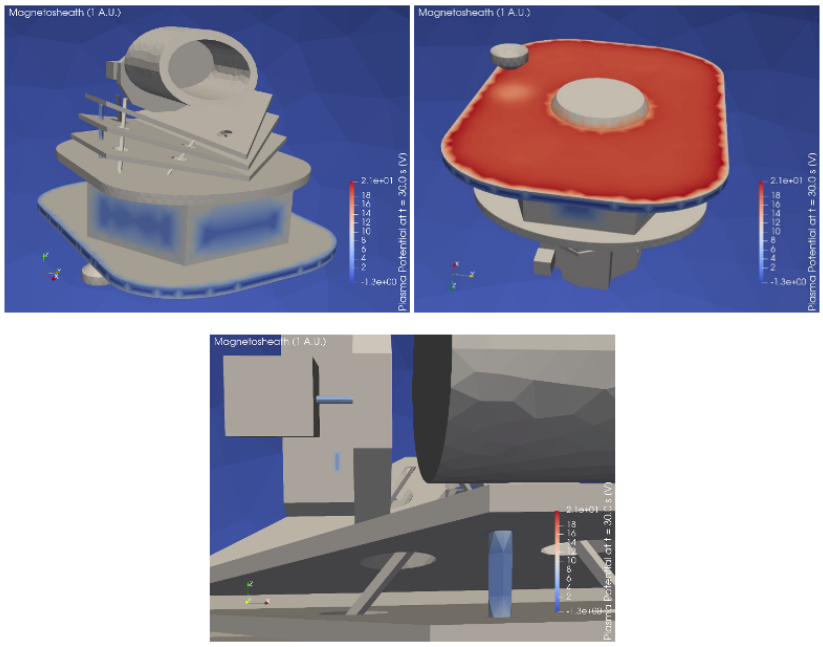

Figure 26: 3D map of plasma potential – Magnetosheath (1 A.U.). First figure: Ariel front; second figure: Ariel bottom; third figure: closeup on FPE-IC connector and FPE strut.

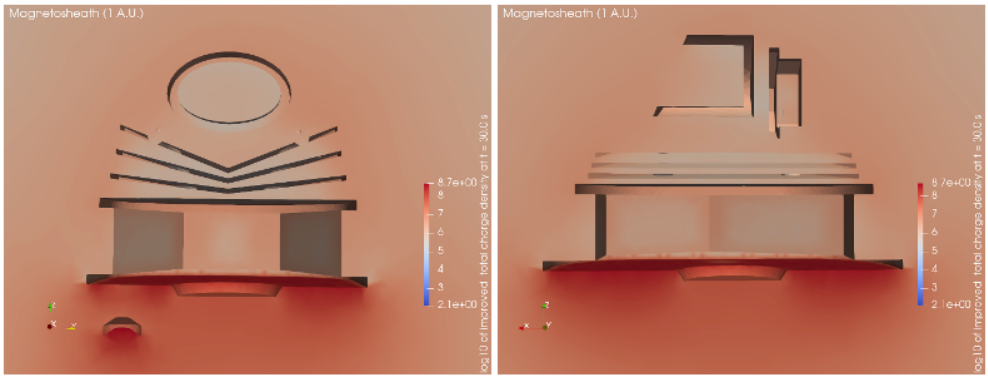

Figure 27: log10 of total charge density (q/m^3) at t = 30.0 s with a cut through the S/C in z-y plane and x-z plane – Magnetosheath.

6.5 1 A.U. Magnetotail

This environment is characterized by the lowest density and higher energy plasma with respect to the other plasma environments encountered by Ariel around L2, causing different potential differences. Being in sunlight, the exposed surfaces will charge positively. The same considerations made for the magnetosheath about having more energetic particles can be replicated in this environment which turns out from literature to be even more energetic and less dense than the previous one.

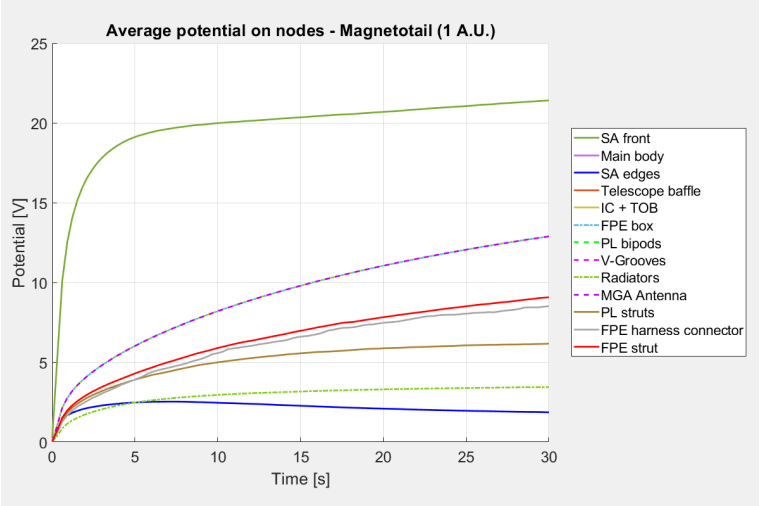

Figure 28: Time dependent surface potential evolution – Magnetotail (1 A.U.).

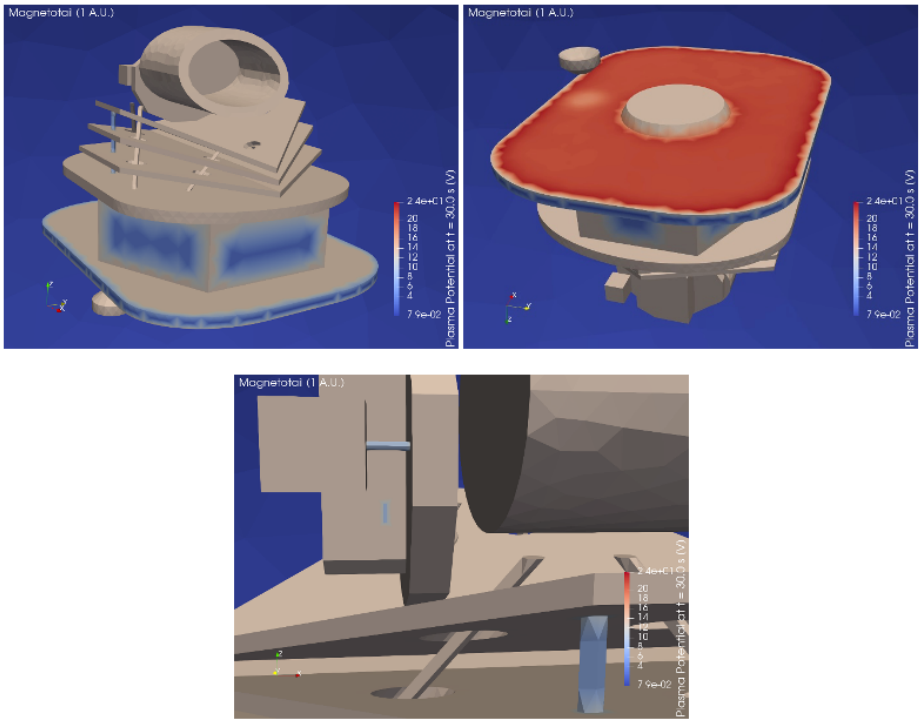

Figure 29: 3D map of plasma potential – Magnetotail (1 A.U.). First figure: Ariel front; second figure: Ariel bottom; third figure: closeup on FPE-IC connector and FPE strut.

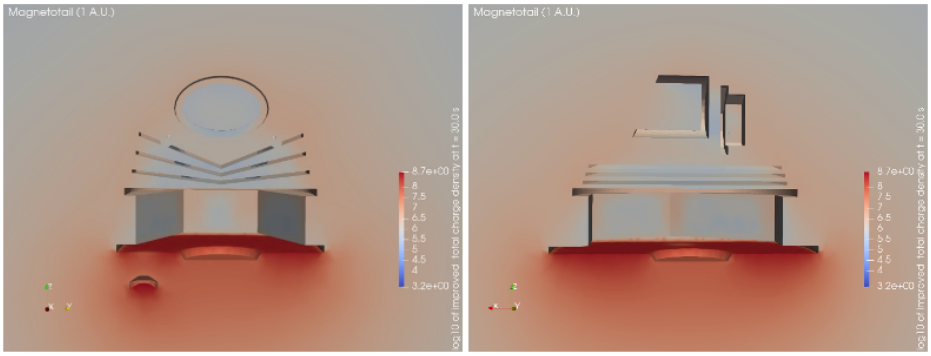

Figure 30: $\log_{10}$ of total charge density (q/m^3) at t = 30.0 s with a cut through the S/C in z-y plane and x-z plane – Magnetotail.

The potential differences between the S/C surfaces are not a cause of concern for ESDs as the biggest voltage difference is about 19.5 V between the Solar Array front, at about 21.5 V and the Solar Array edges, at about 2.0 V. However, the potential differences between the various surfaces, not fully reaching their plateau, may interfere with the on-board instrumentation nominal operation even in the case of small sparkles and ESD, as previously described. Further analysis will be carried out with longer simulation times, as for the solar wind and magnetosheath plasma regimes.

As for the previous cases, this simulation represents a somewhat worst-case scenario.

In Figure 30 the $\log_{10}$ of the total charge density at t = 30.0 s with a cut through the z-y and the x-z planes has been reported.

7. CONCLUSIONS AND FUTURE WORK

This paper has provided an overview on the consolidated surface charging analyses on the Ariel Payload based on simulations carried out by the SPIS simulator. Simulations of net surface charge accumulation on the dielectric and conductive surfaces of the Ariel Payload subsystems were carried out for duration times that allowed a good compromise between reliable results (at least for what concern trends) and reasonable computation times.

It has been shown that in the environments encountered by Ariel in L2 and in LEO orbit there is negligible or no risk of ESDs, in agreement with the threshold value given by the ECSS, according to which the potential difference between two surfaces of the S/C or the potential difference between a surface of the S/C and the plasma must not exceed 100 V. As regards the GEO orbit, instead, voltage difference values of more concern were obtained indicating a possible risk of ESDs.

However, a worst-case scenario has been considered in which the S/C and PL grounding and bonding structures have not been fully implemented and simulated and the dielectric strut surfaces have been considered as not covered by conductive black paint MAP-PUK-AQ. These simulations represent, therefore, a confirmation of the need for such precaution regarding the exposed dielectric material. In addition, a conductive protective cap for the external FPE-IC connector is deemed mandatory, accounting also for the bulk charging risk and expected material degradation due to the full interaction with the space environment (e.g. high energy particles, micrometeoroids, etc.) leading to common precautions ruled by space standards.

Future developments of this work include further simulations with improved computational power to carry out the simulations until all the analyzed surfaces reach their equilibrium (plateau). The creation of a more complex geometry that allows to simulate a larger number of subsystems involved is also planned. One of the future targets is to simulate the passage of the satellite through the Van Allen radiation belts, modelling the worst-case plasma environment by means of the AE8 and AP8 models, accounting for the solar cycle and expected level of solar activity for the actual launch window.

Simulations of transients during which the S/C passes from one environment to another, characterized by strong current sheets and magnetic fields, leading to possibly hazardous variations related to sudden surface potential redistribution, are also planned. This study will then be extended from the mere analysis of surface charging to an in-depth analysis of the

bulk charging phenomenon, especially for the Van Allen radiation belts environment (in particular the external one limited by GEO orbits), thanks to future developments of the dedicated SPIS tool, still in its beta version.

Further details on the overall Payload design and electronic architecture along with its current status can be found in [18] and [19]. A preliminary and a more detailed assessment of Ariel Payload surface charging risk can be respectively retrieved from [20] and [21].

8. ACKNOWLEDGEMENT

The authors would like to thank very much the Ariel Mission Consortium (AMC) and all the involved founding Agencies and Institutions, ESA in particular. A special thanks to UCL – University College of London (UK) leading the Ariel Mission Consortium (AMC) in the person of Prof. Giovanni Tinetti as Ariel Principal Investigator (PI).

This study has been supported by the Italian Space Agency (ASI) thanks to the ASI-INAF agreement n. 2021-5-HH.2-2024 "Scientific activity for the Ariel Mission – B2/C/D1 Phases"

REFERENCES

[1] G. Tinetti et al., "A chemical survey of exoplanets with Ariel", Experimental astronomy (2018).
[2] ESA, "Ariel - Enabling planetary science across light-years", Ariel - Atmospheric Remote-sensing Infrared Exoplanet Large-survey "Red Book," ESA/SCI(2020)1 (November 2020).
[3] E. Pace et al., "The telescope assembly of the Ariel space mission", Proc. SPIE AT&I Conference, Yokohama, Japan – 2024.
[4] K. Skup et al., "Ariel Fine Guidance System: design challenges and opportunities", Proc. SPIE 12180, Space Telescopes and Instrumentation 2022: Optical, Infrared, and Millimeter Wave, 1218013 (27 August 2022).
[5] K. Skup et al., "The Ariel FGS: current design and implementation", Proc. SPIE AT&I Conference, Yokohama, Japan – 2024.
[6] V. Noce et al., "The detector control unit of the fine guidance sensor instrument on-board the Ariel mission: design status", Proc. SPIE 12180, Space Telescopes and Instrumentation 2022: Optical, Infrared, and Millimeter Wave, 1218046 (27 August 2022).
[7] J. Martignac et al., "AIRS: Ariel IR spectrometer status", Proc. SPIE 12180, Space Telescopes and Instrumentation 2022: Optical, Infrared, and Millimeter Wave, 1218012 (27 August 2022).
[8] J. Martignac et al., "Ariel IR Spectrometer development status", Proc. SPIE AT&I Conference, Yokohama, Japan – 2024.
[9] M. Focardi et al., "The Ariel Instrument Control Unit: its role within the Payload and B1 Phase design", Experimental astronomy (2022).
[10] V. Noce et al., "The instrument control unit of the Ariel payload: design evolution following the unit and payload subsystems SRR (system requirements review)", Proc. SPIE 12180, Space Telescopes and Instrumentation 2022: Optical, Infrared, and Millimeter Wave, 1218043 (27 August 2022).
[11] V. Noce et al., "The Instrument Control Unit of the AIRS instrument on-board the Ariel mission: design status after PDR", Proc. SPIE AT&I Conference, Yokohama, Japan – 2024.
[12] CREMA – "Consolidated Report on Mission Analysis", Issue 1, Revision 0, ESA-ARIEL-ESOC-MIS-RP-001 by B. De Vogeleer, F. Renk - April 2019
[13] SPINE and SPIS Suite - www.spis.org
[14] *Ariel Environment Specification*, D. Rodgers et al., ESA-Ariel-EST-SP-001, 2018.
[15] ECSS-E-ST-10-04-C Rev. 1, Space environment, 2020.
[16] ECSS-E-ST-20-06C Rev.1, Spacecraft Charging, 2019.
[17] *Fundamentals of Spacecraft Charging*, Princeton University Press, Shu T. Lai, 2011.
[18] P. Eccleston and the Ariel Mission Consortium, "The Ariel payload design post-PDR", Proc.SPIE AT&I Conference, Yokohama, Japan – 2024.
[19] M. Focardi and the Ariel Mission Consortium, "An overview of the electrical, electronic and on-board data handling architecture of the Ariel Payload", EDHPC Conference, Juan Le Pins, France – 2023.
[20] *Preliminary surface charging analysis of the Ariel Payload dielectrics in early transfer orbit and L2-relevant space environment*, M. Focardi et al., SPIE Proc., 2022.
[21] *Ariel charging analysis: effects of space plasma environments along the spacecraft orbit*, M. Michelagnoli, Physics Degree Thesis work, University of Florence - Italy, 2024.